

Supplementary Information

Modeling Thermocatalytic Systems for CO₂ Hydrogenation to Methanol

Jikai Sun and Jianzhong Wu

*Department of Chemical and Environmental Engineering, University of California, Riverside,
CA 92521, USA*

1. Electronic DFT calculation

The atomic configurations and electronic energies of CO₂ and CO hydrogenation process on Cu (111) and Cu (211) surfaces were obtained by Shi et al.¹ These authors demonstrated that hydrogen molecules on the Cu surface readily dissociate at high temperature ($E_{\text{barrier}} = 0.56$ eV on Cu (111), and $E_{\text{barrier}} = 0.69$ eV on Cu (211)), thereby allowing for the direct addition of hydrogen atoms along the reaction pathway.

The low-energy pathways shown in Figure 2 were identified by utilizing a microkinetics-guided machine learning pathway search (MMLPs) method and further optimized by KS-DFT calculations.¹ In this study, we did not consider the influence of the gas-phase environment on the surface geometry. Therefore, KS-DFT and cDFT calculations are independent of each other. The DFT-optimized structures and their corresponding energies, except for the energy of the *H+CO₂ structure, were directly adopted from Shi et al.¹ Because CO₂ is often considered non-adsorbed on the Cu surface, Shi et al. calculated relative to the gas-phase CO₂ energy. This approach resulted in energy barriers of 0.69 eV on Cu (111) and 0.53 eV on Cu (211) for the CO₂+H* → HCOO* reaction. In contrast, we calculated the energy barriers relative to the *H+CO₂ structure, obtaining values of 0.99 eV on Cu (111) and 0.86 eV on Cu

(211). The energies of all other structures are consistent with those reported in their work. This method can be extended to any gas-phase reaction system, leveraging existing DFT structures and energy landscapes.

In the calculation of entropy correction, the vibration analysis were conducted using the PBE functional of the GGA method as implemented in the CP2K package.² To minimize basis set superposition errors, the wave functions were expanded in the DZVP-MOLOPT-SR-GTH basis set^{3,4} along with the cutoff energy of 450 Ry for the auxiliary plane-wave basis set. Core electrons were modeled by the Geodecker-Teter-Hutter (GTH) pseudopotentials.⁵⁻⁷ The wavefunction convergence was ensured with an SCF tolerance of 10^{-6} . The DFT-D3 method proposed by Grimme⁸ was added to correct the intermolecular van der Waals (vdW) interaction among surface atoms. Since the grid precision has limited effect on vibration analysis, only the Γ -point approximation was employed to sample the Brillouin zone.⁹

The free energy of the intermediates at different temperatures were analyzed through Shermo package¹⁰ based on the vibration information.

2. Grand potential theory

The computational box was divided into two subsystems: one includes the catalyst with chemically adsorbed species, and the other consists of the environmental gas molecules. The grand potential of the entire system was calculated from:

$$\Omega = E_{KS-DFT} + G_{corr} + \Omega_{cDFT} \quad (1)$$

where E_{KS-DFT} and G_{corr} represent the ground-state energy and the free-energy correction for bond vibrations of the catalyst and surface species, respectively, and Ω_{cDFT} represents the grand

potential of the environmental gas molecules. While E_{KS-DFT} and G_{corr} are obtained from KS-DFT calculations, Ω_{cDFT} was calculated using classical density functional theory (cDFT), which also provides the density profiles of all gas-phase components around the catalyst surface at specified temperatures and pressures.

The cDFT simulations were carried out using our in-house developed GPU-accelerated cDFT package, assuming that gas molecules can be represented by the Lennard-Jones (LJ) model¹¹. It has demonstrated in our previous work that the cDFT method is both highly efficient and accurate in simulating gas adsorption on surfaces and in nanoporous materials.^{12,13} Briefly, the thermodynamic properties of gas molecules near a catalytic surface are derived from the grand potential^{12,14,15}:

$$\Omega_{cDFT} = F[\rho_i(r)] + \sum_i \int [V_i^{ext}(R,r) - \mu_i] \rho_i(r) dr \quad (2)$$

where $F[\rho_i(r)]$ represents the intrinsic Helmholtz energy, and $V_i^{ext}(R,r)$ is the external potential of gas species i , and μ_i is the chemical potential. In this work, the external potential corresponds to the energy experienced by each gas molecule due to its interaction with the surface atoms. More specifically, $V_i^{ext}(R,r)$ describes the interaction of a gas molecule at position r with the catalyst and chemically adsorbed species. The configuration R is defined by the atomic positions of the catalyst and chemically adsorbed surface species.

The interaction energy between each surface atom and a gas molecule is also given by the LJ potential

$$V_{LJ}(r) = 4\varepsilon \left[\left(\frac{\sigma}{r} \right)^{12} - \left(\frac{\sigma}{r} \right)^6 \right] \quad (3)$$

where ε and σ are the energy and size parameters, and r is the distance between the gas

molecule and the surface atom. The LJ potential parameters, including those for gas-gas interactions, are listed in Table S1. The Lorentz-Berthelot mixing rules are used for interactions between different species. These parameters are crucial for accurately representing the interactions between the gas molecules and the catalyst surface.

To calculate the chemical potential of the bulk phase, we utilized the modified Benedict–Webb–Rubin (MBWR) equation of state, which is well-suited for gas-phase systems under various conditions of temperature and pressure.¹⁶ While the MBWR equation of state and LJ potential are typically designed for gas-phase molecules, not for polar molecules such as H₂O, our simulations were performed at high temperatures and low partial pressures of water vapor. In these conditions, the focus of our analysis is primarily on the dispersion interaction of H₂O molecules with nonpolar gas and surface species, rather than on interactions between H₂O molecules. This simplification is justified given the low H₂O density and high temperature, where the gas-phase behavior is less significant compared to the solid-gas interface interactions.

For adsorption energy calculations using KS-DFT, we follow the conventional method

$$E_{ad} = E_{*species} - E_{*} - u_{species} \quad (4)$$

where $E_{*species}$, E_{*} , and $u_{species}$ represent the energies of the catalyst with the adsorbates, the pristine catalyst, and the gas-phase adsorbate molecules, respectively. To determine the Gibbs energy of adsorption, entropy correction is applied to the adsorbate molecules due to the changes in bond vibrations before and after adsorption.

In the calculation of the grand-potential adsorption energy (Ω_{ad}), we need to consider the gas phase explicitly. In this case, both the pristine catalyst and the catalyst with the adsorbates

are influenced by the presence of gas molecules in the bulk phase. The grand-potential adsorption energy is defined as

$$\Omega_{ad} = \Omega_{*species} - \Omega_{*} - u_{species} \quad (5)$$

In the grand-potential approach, the reference state is defined in terms of the bare surface in contact with the gas phase under the reaction condition. As shown in Fig. S1 for the co-adsorption of CO₂ and H*, the presence of intermediate species at the surface (viz., adsorbates) blocks the physical adsorption of gas-phase species, resulting in an increase of the grand potential.

Substituting Eq. (1) into (5) gives the grand potential correction of the adsorption energy

$$\Omega_{ad-corr} = \Omega_{ad} - G_{ad} = \Omega_{cDFT-*species} - \Omega_{cDFT-*} \quad (6)$$

where $\Omega_{cDFT-*species}$ is the grand potential of the system at an intermediate state, i.e., the gas phase in contact with the catalyst with the adsorbates, and Ω_{cDFT-*} corresponds to that of the same gas system but in contact with the pristine catalyst. While the electronic properties of the catalyst and adsorbates are predicted with KS-DFT, we use cDFT to describe the thermodynamic properties of the inhomogeneous gas system using the LJ model. Because we use a pristine catalyst in contact with a gas phase as the reference, the grand potential adsorption energy is much larger than those obtained from the conventional KS-DFT calculations. The external energy of the gas phase changes significantly when the Cu surface is occupied by the adsorbates, leading to significant increase of the surface energy (up to 10 kcal/mol) in $\Omega_{ad-corr}$. Intuitively, $\Omega_{ad-corr}$ can be understood as the energy associated with the reduction of attraction energy between gas-phase species and Cu atoms.

After obtaining the grand potential (Ω) for each reaction intermediate, we calculated the

reaction energy barrier in the grand potential framework (Ω_b) based on the following equation:

$$\Omega_b = \Omega_{TS} - \Omega_{IS} = E_b + G_{b-corr} + \Omega_{b-corr} \quad (7)$$

where Ω_{b-corr} is the grand potential correction term (Eq. S6), defined as:

$$\Omega_{b-corr} = \Omega_{cDFT-TS} - \Omega_{cDFT-IS} = \Delta\Omega \quad (8)$$

This means that compared to the free energy barrier (G_b), the grand potential barrier (Ω_b) includes an additional correction term accounting for the effect of the surface interaction with the surrounding environment.

3. Transition State Theory (TST)

3.1 Conventional DFT approach

According to the transition state theory (TST)¹⁷, the rate constant k_i for each surface reaction can be expressed as:

$$k_i = \frac{k_B T}{h} e^{\frac{-\Delta G}{k_B T}} \quad (9)$$

where ΔG represent the energy barrier after the correction for the bond vibration entropy of the substrate. The reaction equilibrium constant $K_i = \frac{k_{i,f}}{k_{i,r}}$ is related to the ratio of the forward $k_{i,f}$ and reverse reaction rate constants $k_{i,r}$.

Two surface reactions were under consideration in this work:



The rate for Reaction R1 can be expressed as:

$$r_1 = k_{1,f} P_{\text{CO}_2} \theta_* P_{\text{H}} - k_{1,r} \theta_{\text{HCOO}^*} \quad (10)$$

where P_{CO_2} and P_H are the partial pressures of CO_2 and hydrogen atoms in the gas phase, respectively, and θ_{HCOO^*} is the surface coverage of the $HCOO^*$ intermediate. Assuming that the hydrogenation of $HCOO^*$ is the rate determining step, we can estimate the $HCOO^*$ coverage based on quasi-equilibrium, $r_1 = 0$.¹⁸ The corresponding equilibrium coverage becomes:

$$\theta_{HCOO^*} = \frac{k_{1,f} P_{CO_2} P_H}{k_{1,r}} \theta_* \quad (11)$$

Given that $\theta_* + \theta_{HCOO^*} \approx 1$, the above expression simplifies to:

$$\theta_{HCOO^*} = \frac{K_1 P_{CO_2} P_H}{1 + K_1 P_{CO_2} P_H} \quad (12)$$

Thus, the forward rate of $HCOO^*$ hydrogenation can be calculated from:

$$r_{2,f} = \theta_{HCOO^*} P_H k_{2,f} = \theta_{HCOO^*} P_H \frac{k_B T}{h} e^{\frac{-\Delta E_{HCOO^*}}{k_B T}} \quad (13)$$

3.2 The grand potential theory

In the grand potential theory, the reaction rate depends on the grand potential barrier and surface densities. In this case, the rate constant k_i for each surface reaction can be rewritten as:

$$k_i = \frac{k_B T}{h} e^{\frac{-\Delta\Omega}{k_B T}} \quad (14)$$

where $\Delta\Omega$ represent the grand-potential barrier. The rate for Reaction R1 can be rewritten as:

$$r_1 = k_{1,f} \rho_{s,CO_2} \theta_* \rho_{s,H} - k_{1,r} \theta_{HCOO^*} \quad (15)$$

where ρ_{s,CO_2} and $\rho_{s,H}$ are the surface densities of CO_2 and hydrogen atoms, respectively. Thus, the quasi-equilibrium assumption for reaction R1 leads to the $HCOO^*$ surface coverage

$$\theta_{HCOO^*} = \frac{K_1 \rho_{s,CO_2} \rho_{s,H}}{1 + K_1 \rho_{s,CO_2} \rho_{s,H}} \quad (16)$$

The forward rate of HCOO* hydrogenation is then calculated from:

$$r_{2,f} = \theta_{HCOO^*} \rho_{s,H} k_{2,f} = \frac{K_1 \rho_{s,CO_2} \rho_{s,H}}{1 + K_1 \rho_{s,CO_2} \rho_{s,H}} \rho_{s,H} \frac{k_B T}{h} e^{\frac{-\Delta\Omega_{HCOO^*}}{k_B T}} \quad (17)$$

Table S1 The Lennard-Jones parameters for gas molecules and element atoms considered in this work.

Species	ϵ (K)	σ (Å)	ref
H ₂	36.7	2.96	11
CO ₂	200.9	3.943	19
CO	104.5	3.698	19
H ₂ O	506.0	2.71	19
Cu	4750	2.338	20
C	52.85	3.851	21
H	22.14	2.886	21
O	30.20	3.50	21

Table S2 Free energy correction of key species in CO₂ and CO hydrogenation on Cu (111) and Cu (211) surface at different temperatures.

Species / T (K)	Cu (111)					Cu (211)				
	303	403	503	603	703	303	403	503	603	703
H*	3.64	3.55	3.38	3.15	2.84	3.79	3.70	3.53	3.30	3.00
TS-CO ₂	9.06	8.50	7.71	6.72	5.54	10.28	9.62	8.71	7.57	6.22
HCOO*	12.82	12.33	11.68	10.87	9.91	13.19	12.29	11.15	9.76	8.17
TS-HCOO*	17.21	16.06	14.61	12.86	10.84	16.38	15.47	14.27	12.79	11.05
HCOOH*	21.67	20.86	19.82	18.56	17.08	21.05	20.16	18.98	17.53	15.81
TS-HCOOH*	23.69	22.67	21.25	19.45	17.31	22.01	21.26	20.24	18.95	17.40
H ₂ COOH*	27.38	26.51	25.33	23.86	22.11	27.20	26.33	25.15	23.67	21.91
TS- H ₂ COOH*	24.43	23.37	21.99	20.31	18.36	25.69	24.45	22.84	20.88	18.60
HCHO*	18.05	17.24	16.23	15.03	13.66	16.82	16.04	15.04	13.85	12.47
TS-HCHO*	19.80	19.10	18.14	16.92	15.47	19.70	18.95	17.93	16.67	15.17
CH ₃ O*	24.60	23.78	22.71	21.41	19.88	24.41	24.04	23.50	22.81	21.95

TS-CH3O*	29.43	28.76	27.90	26.84	25.58	28.31	27.42	26.26	24.84	23.16
CH3OH*	35.28	34.59	33.64	32.45	31.00	31.85	30.98	29.89	28.56	27.02
CO*	8.30	7.41	6.25	4.84	3.21	9.53	8.82	7.85	6.64	5.21
TS-CO*	6.57	5.79	4.78	3.58	2.20	7.16	6.60	5.83	4.87	3.73
CHO*	9.60	8.77	7.72	6.47	5.04	9.97	9.46	8.78	7.93	6.93

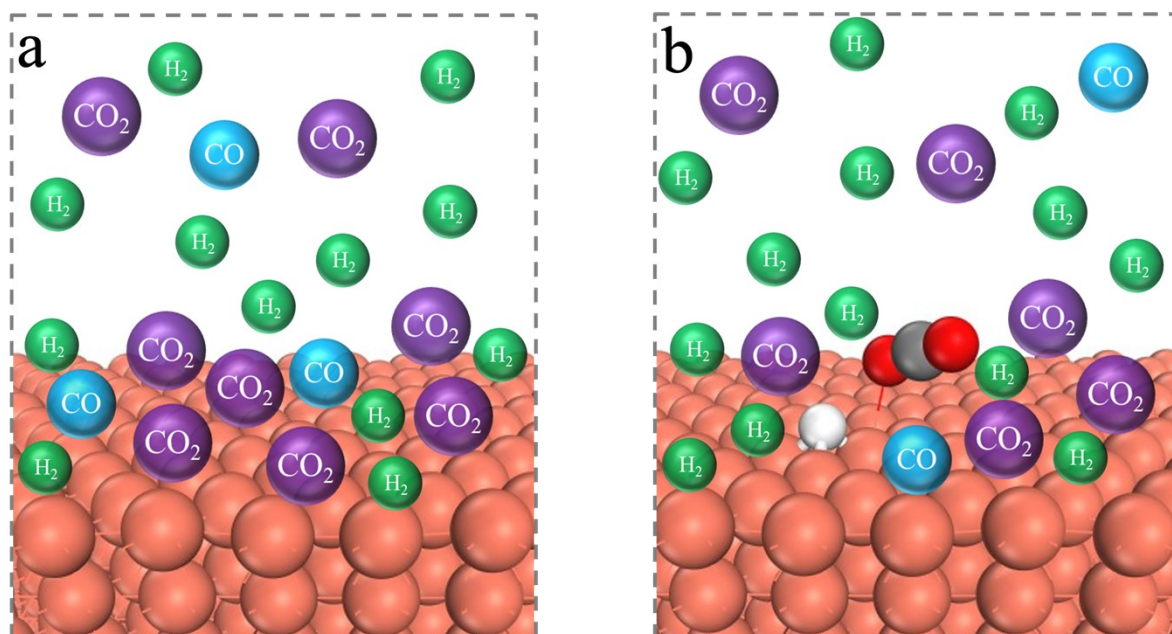


Fig. S1. Schematic illustrations of the grand-potential method to calculate the adsorption energy. a) The reference state is defined as a pristine catalyst surface in contact with the gas phase. Here, the purple, blue, and green spheres represent CO_2 , CO , and H_2 in the gas phase, respectively, as described by the Lennard-Jones model. b) The catalyst surface and adsorbates, $\text{CO}_2 + \text{H}^*$, surrounded by molecules from the bulk phase. The hydrogen atom is positioned at the hollow site of the copper surface, and a CO_2 molecule is weakly attached to a Cu atom nearby.

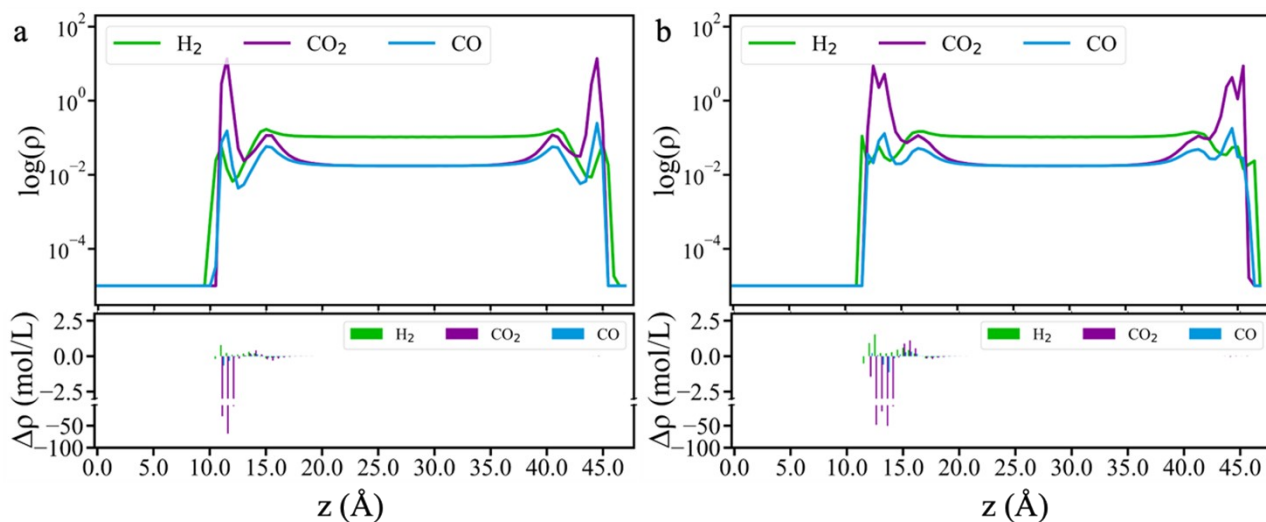


Fig. S2. Average gas densities along the direction (z -axis) perpendicular to Cu (111) (a) and Cu (211) (b) surfaces. Below: the variation of the local densities due to the chemical adsorption

of HCOO^*-H^* intermediates at the copper surfaces, $\Delta\rho = \rho_{\text{HCOO}^*-\text{H}^*} - \rho_{\text{bare}}$.

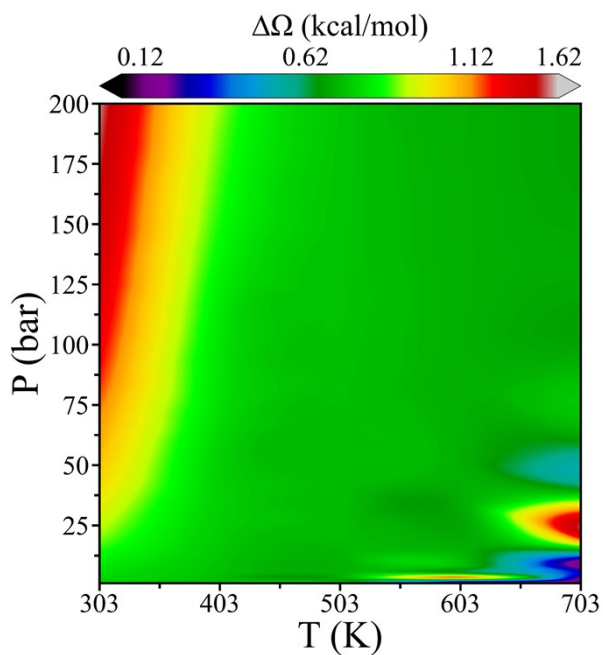


Fig. S3. Contour plot of the change in grand potential barrier as a function of temperature and pressure for HCOOH^* hydrogenation on Cu (111) surfaces.

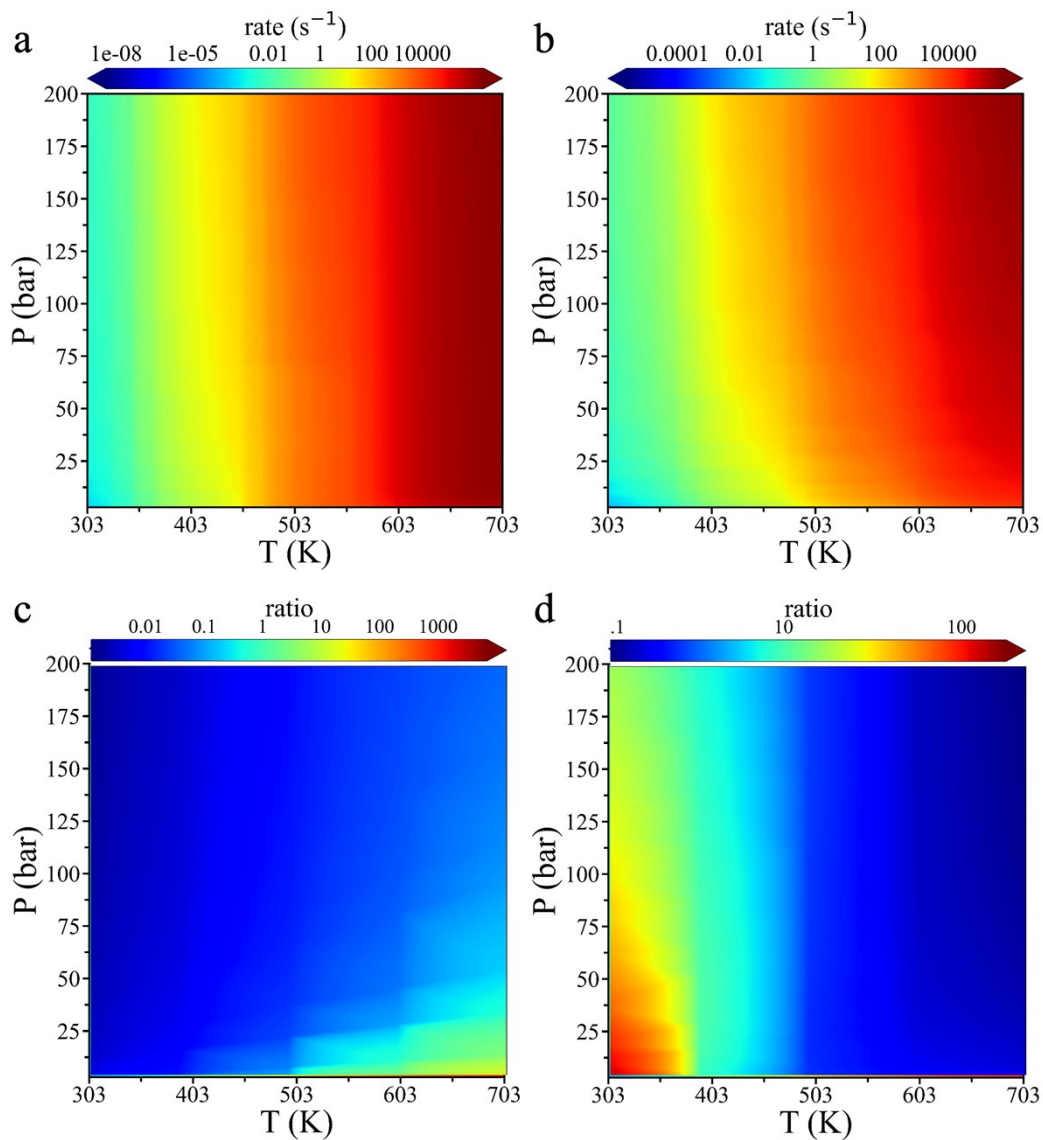


Fig. S4. Contour plots of the HCOO* hydrogenation rates obtained from grand potential simulations as functions of temperature and pressure on Cu (111) (a) and Cu (211) (b) surfaces. The corresponding ratios of the rates obtained from grand potential and surface density to those obtained from free energy and bulk density are presented in (c) and (d).

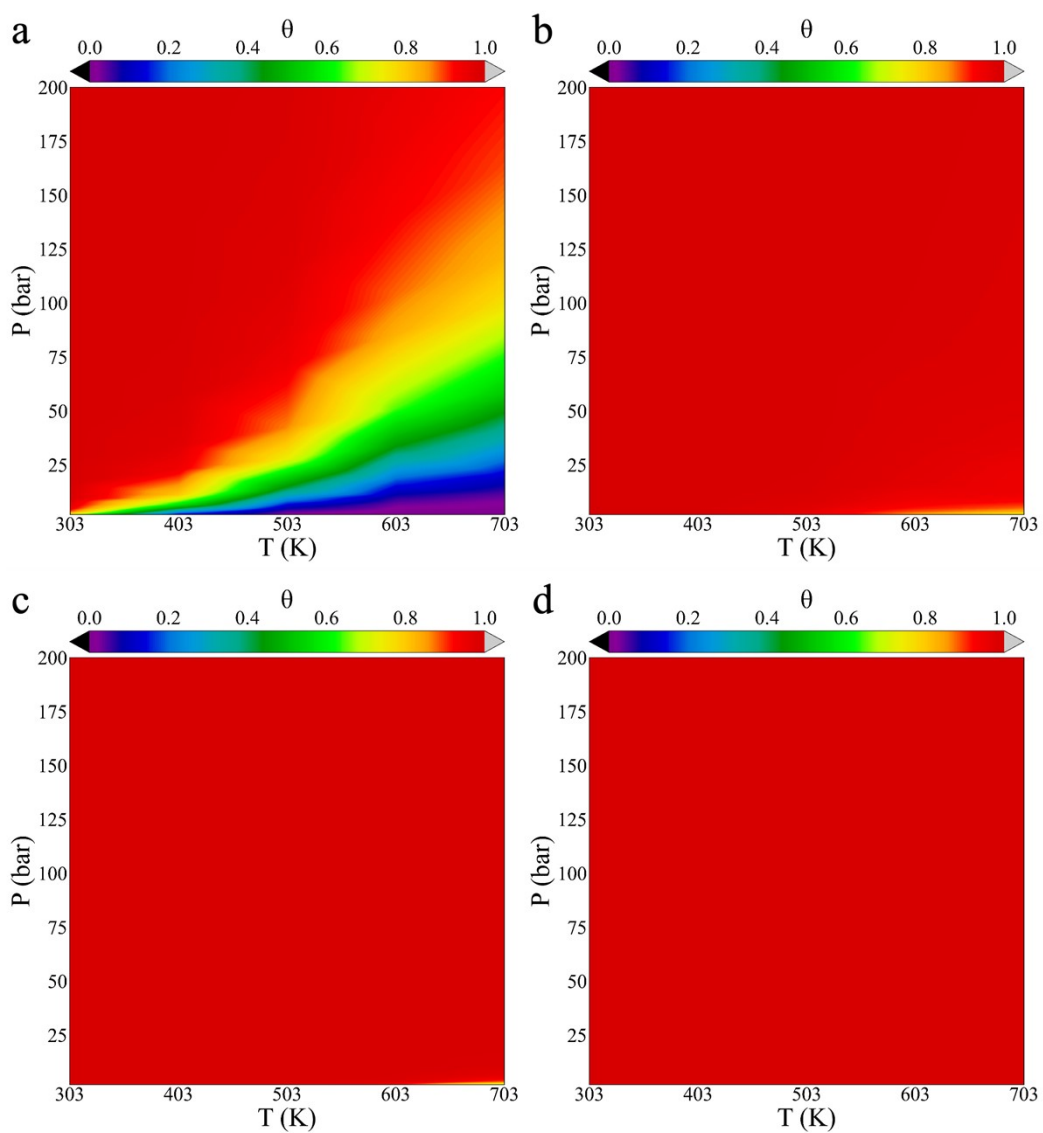


Fig. S5. Contour plots of the HCOO* coverage (θ) on Cu (111) (a) and Cu (211) (c) surfaces versus temperature and pressure obtained from conventional DFT approach. The surface coverage on Cu (111) (b) and Cu (211) (d) obtained from the grand potential theory.

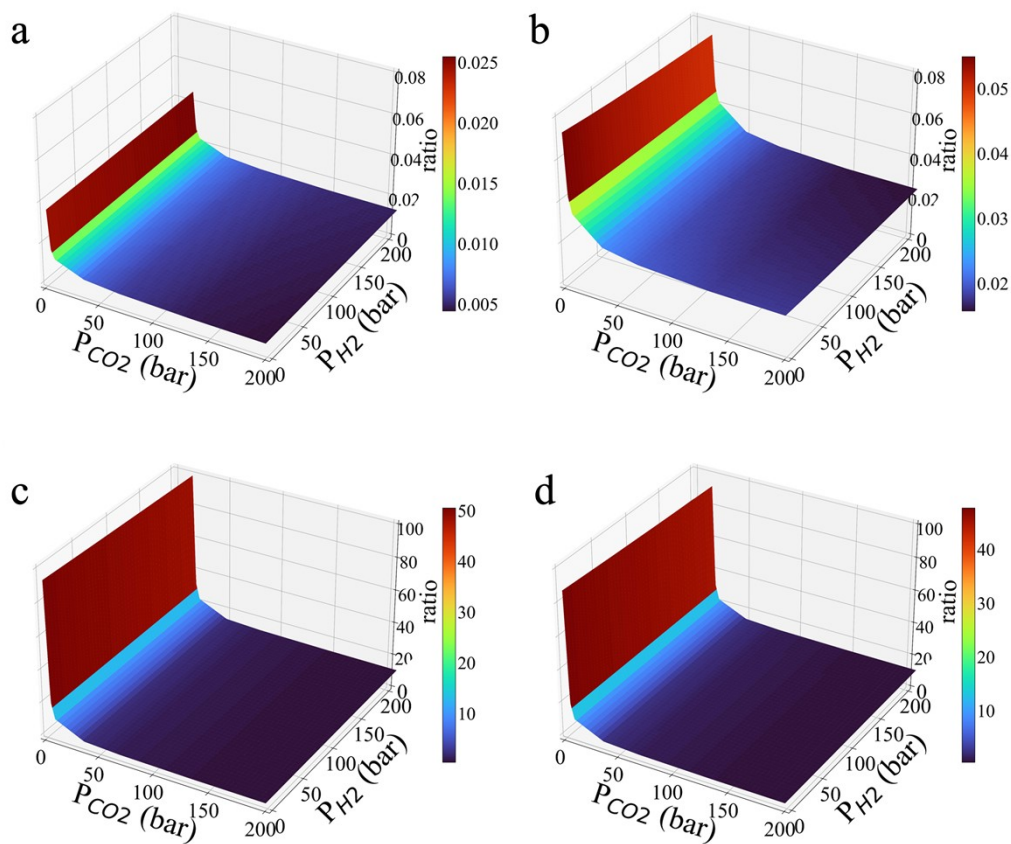


Fig. S6. Density maps showing the ratio of surface density to bulk density for H_2 on Cu (111) (a) and Cu (211) (b) surfaces, as well as for CO_2 on Cu (111) (c) and Cu (211) (d) surfaces. These ratios are presented as functions of H_2 and CO_2 partial pressures.

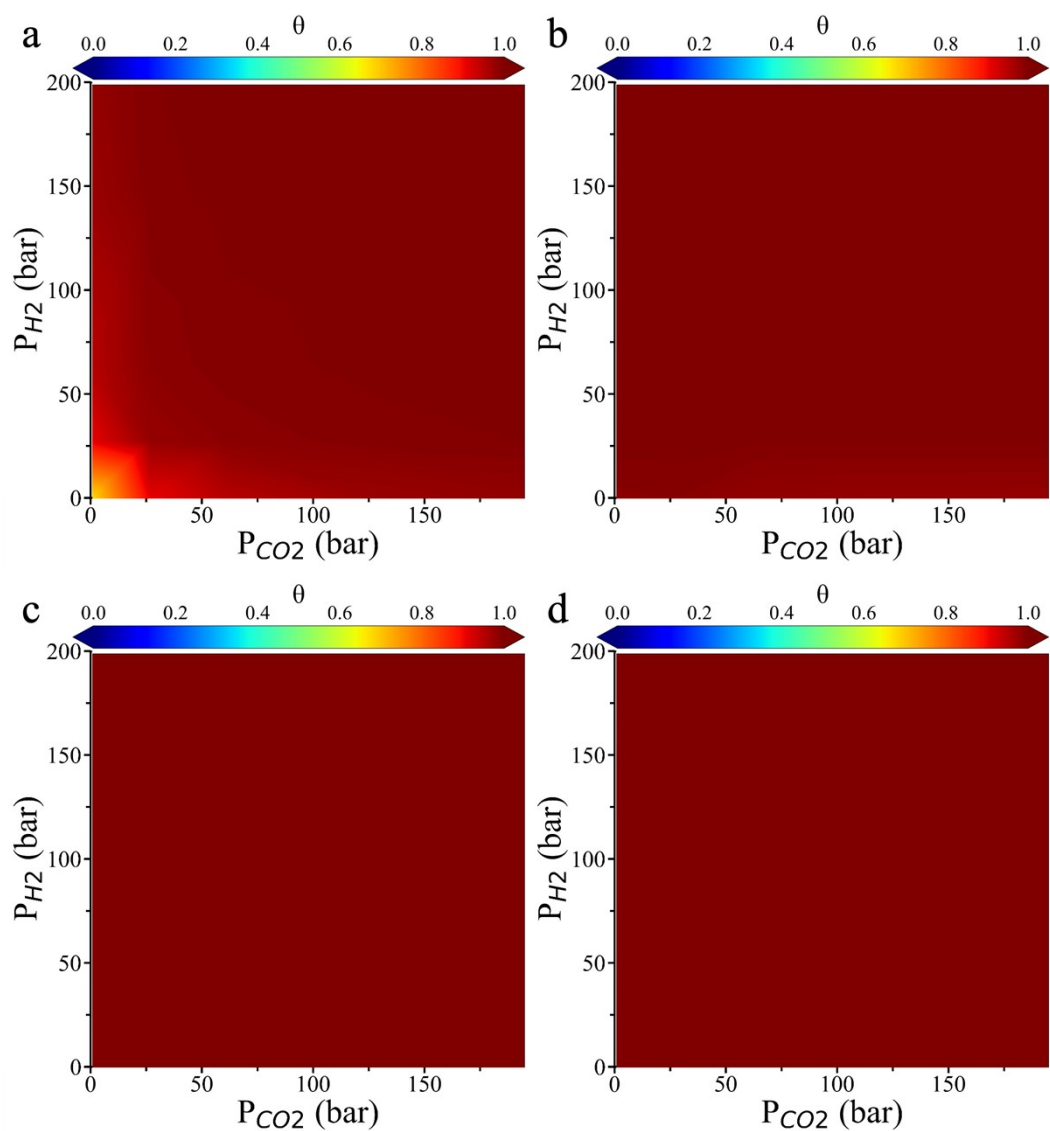


Fig. S7. Contour plots of the HCOO* coverage (θ) on Cu (111) (a) and Cu (211) (c) surfaces versus H₂ and CO₂ partial pressure obtained from conventional DFT approach. The surface coverage on Cu (111) (b) and Cu (211) (d) obtained from the grand potential theory.

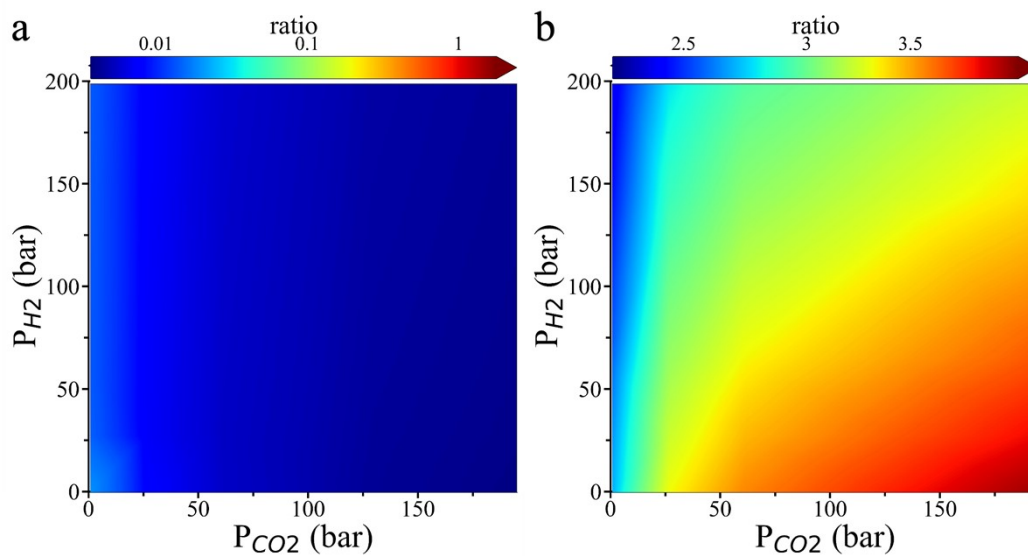


Fig. S8. The ratios of the HCOO* hydrogenation rates obtained from grand potential and surface density to those obtained from free energy and bulk density on Cu (111) (a) and Cu (211) (b) surface as functions of H₂ and CO₂ partial pressure.

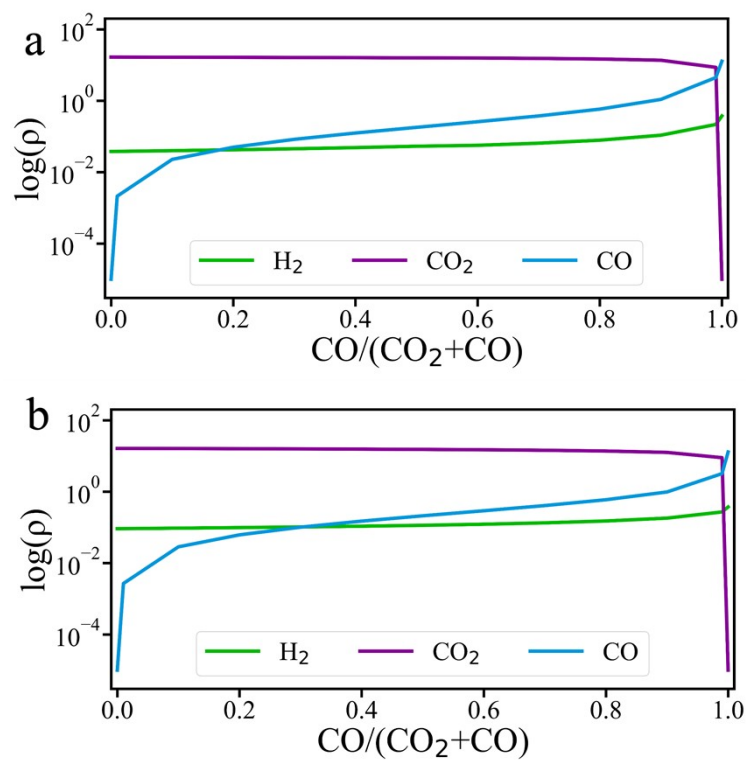


Fig. S9. Surface densities of the feed gas with the CO/(CO₂ + CO) ratio on Cu (111) (a) and Cu (211) (b) surfaces at an H₂ pressure of 8 bar. All simulations were conducted at 503 K, with a fixed feed gas ratio of H₂:(CO₂ + CO) = 3:1.

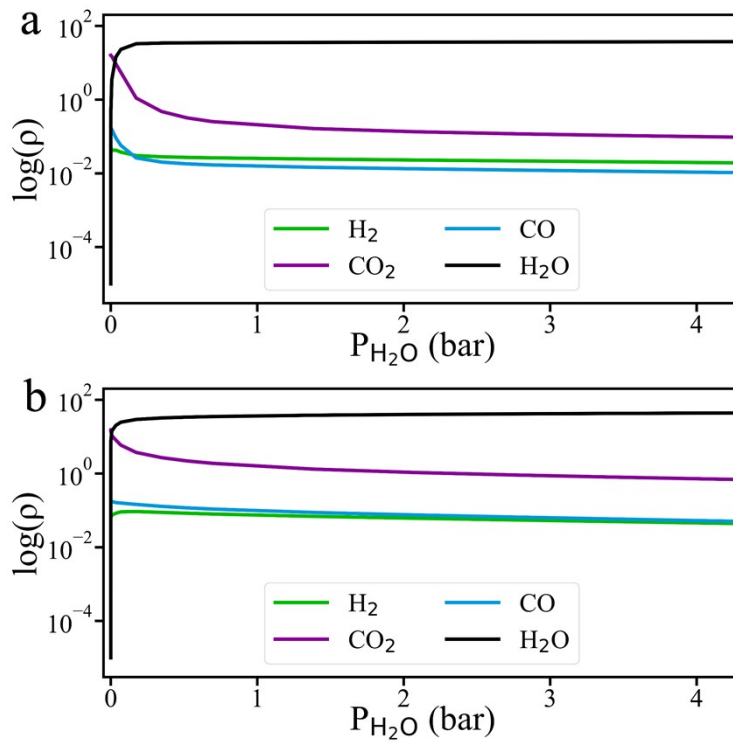


Fig. S10. Surface densities of the feed gas with varying H_2O partial pressures on Cu (111) (a) and Cu (211) (b) surfaces at an H_2 pressure of 8 bar. All simulations were conducted at 503 K, with a fixed feed gas ratio of $\text{H}_2:\text{CO}_2:\text{CO} = 6:1:1$.

Reference

- 1 Y.-F. Shi, P.-L. Kang, C. Shang and Z.-P. Liu, *J. Am. Chem. Soc.*, 2022, **144**, 13401–13414.
- 2 J. Hutter, M. Iannuzzi, F. Schiffmann and J. VandeVondele, *Wiley Interdiscip. Rev. Comput. Mol. Sci.*, 2014, **4**, 15–25.
- 3 J. VandeVondele and J. Hutter, *J. Chem. Phys.*, 2007, **127**, 114105.
- 4 J. VandeVondele, M. Krack, F. Mohamed, M. Parrinello, T. Chassaing and J. Hutter, *Comput. Phys. Commun.*, 2005, **167**, 103–128.
- 5 S. Goedecker, M. Teter and J. Hutter, *Phys. Rev. B*, 1996, **54**, 1703–1710.
- 6 C. Hartwigsen, S. Goedecker and J. Hutter, *Phys. Rev. B*, 1998, **58**, 3641–3662.
- 7 M. Krack, *Theor. Chem. Acc.*, 2005, **114**, 145–152.
- 8 S. Grimme, S. Ehrlich and L. Goerigk, *J. Comput. Chem.*, 2011, **32**, 1456–1465.
- 9 H. J. Monkhorst and J. D. Pack, *Phys. Rev. B*, 1976, **13**, 5188–5192.
- 10 T. Lu and Q. Chen, *Comput. Theor. Chem.*, 2021, **1200**, 113249.
- 11 M. Zhou and J. Wu, *J. Chem. Phys.*, 2020, **153**, 074101.
- 12 M. Zhou and J. Wu, *Npj Comput. Mater.*, 2022, **8**, 256.
- 13 M. Zhou, Y. Tian, W. Fei and J. Wu, *J. Phys. Chem. C*, 2019, **123**, 7397–7407.
- 14 M. Zhou, A. Vassallo and J. Wu, *J. Membr. Sci.*, 2020, **598**, 117675.
- 15 M. Zhou, J. Wang, J. Garcia, Y. Liu and J. Wu, *Ind. Eng. Chem. Res.*, 2021, **60**, 17016–17025.
- 16 J. K. Johnson, J. A. Zollweg and K. E. Gubbins, *Mol. Phys.*, 1993, **78**, 591–618.
- 17 B. Peters, in *Reaction Rate Theory and Rare Events Simulations*, ed. B. Peters, Elsevier, Amsterdam, 2017, pp. 227–271.
- 18 Y. Wang, J. Yang, Y. Sun, D. Ye, B. Shan, S. C. E. Tsang and X. Tu, *Chem*, 2024, **10**, 2590–2606.
- 19 F. M. Mourits and F. H. A. Rummens, *Can. J. Chem.*, 1977, **55**, 3007–3020.
- 20 T. Halicioğlu and G. M. Pound, *Phys. Status Solidi A*, 1975, **30**, 619–623.
- 21 A. K. Rappe, C. J. Casewit, K. S. Colwell, W. A. Goddard and W. M. Skiff, *J. Am. Chem. Soc.*, 1992, **114**, 10024–10035.